THE JOURNAL OF PHYSICAL CHEMISTRY C

Article

Cite This: J. Phys. Chem. C 2018, 122, 23574−23581

pubs.acs.org/JPCC

Observing Chemical Reactions by Time-Resolved High-Resolution Neutron Imaging

Jasmin Terreni,[†,‡] Matthias Trottmann,[†] Renaud Delmelle,[§] Andre Heel,[§] Pavel Trtik,[∥] Eberhard H. Lehmann,[∥] and Andreas Borgschulte*[,†,‡]

[†]Laboratory for Advanced Analytical Technologies, Empa, Swiss Federal Laboratories for Materials Science and Technology, Überlandstrasse 129, CH-8600 Dübendorf, Switzerland

[‡]Department of Chemistry, University of Zürich, Winterthurerstrasse 190, CH-8057 Zürich, Switzerland

[§]ZHAW—Zürcher Hochschule für Angewandte Wissenschaften, Institute of Materials and Process Engineering (IMPE), Technikumstrasse 9, CH-8400 Winterthur, Switzerland

[∥]Laboratory for Neutron Scattering and Imaging (LNS), Paul Scherrer Institut (PSI), CH-5232 Villigen PSI, Switzerland

Supporting Information

ABSTRACT: We developed an *operando* technique based on time-resolved high-resolution neutron imaging to map the water concentration distribution inside millimeter-sized catalyst beads catalyzing the sorption-enhanced CO_2 methanation reaction. By combining the spatially resolved results from neutron microscopy with the space-integrated reaction kinetics by gas analysis, we are able to study the reaction kinetics including production rates of molecules and mass transport on the mesoscale. We find that the diffusion of water through catalysts is a critical reaction constraint for the sorption-enhanced methanation reaction. We derive the Thiele parameter of a technical catalyst as a quantitative measure, supporting the materials and reactor design of sorption-enhanced methanation. From this, we conclude that nanostructuring sorption catalysts to shorten the diffusion pathway is advantageous over physical mixtures of macroscopic sorbents and catalysts, resulting in long diffusion path lengths. Water accumulation inducing a neutron contrast is specific to a few sorption-enhanced reactions. To extend the applicability of the method to other catalytic systems without sorption enhancement, we introduce a combination of neutron microscopy with steady-state isotopic transient kinetic analysis: hydrogen−deuterium exchange as a measure of the catalytic activity can be followed by neutron imaging.

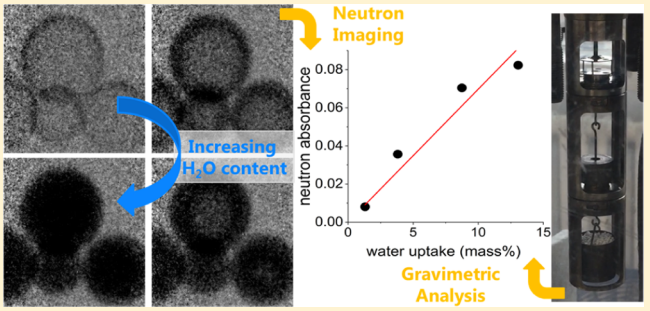

INTRODUCTION

The performance of heterogeneous catalysis relies on the functioning and availability of highly active surface sites with high conversion rate and selectivity for the desired reaction.[1,2] Research and development in heterogeneous catalysis focuses on designing and optimizing these sites. However, the industrial success of a catalyst is based on the fact that a structure ("support") exists, which hosts these sites, and guarantees the mass transport of reactants and products to and from the active sites, respectively. Typical examples are catalyst pellets/beads made of aggregates of a crystalline oxide support with the catalytically active metallic nanoparticles.[3] The support prevents the growth of nanometer-sized particles. The micrometer-sized composites are assembled to millimeter-sized beads for improved external mass transport in the reactor (low pressure loss in large-scale production plants). The setup of such an industrial catalyst must be optimized on the microscopic as well as macroscopic level. The effective concentration of the reacting species at the catalytically active site is limited by the diffusion mechanism and path of reactants and products through the catalyst. To quantify this dependency in technical catalysts, as early as 1939, Thiele introduced a modulus h_T[4−6]

$$h_T^2 = \frac{\text{reaction rate}}{\text{diffusion rate}} \quad (1)$$

which assumes large values, if the reaction rate is much higher than the diffusion rate. Consequently, diffusion dominates the overall conversion. If the reaction is much slower than diffusion, the reaction dominates the overall conversion. In any catalyst, the reaction rates are reduced by diffusion; however, mass transport limitations are unavoidable in practice, that is, in a macroscopic reactor. Furthermore, as the diffusion mechanism is specific to the compounds involved, the microscopic structure may define the selectivity of the process.[7−9] Despite the obvious scientific link between the mesoscopic structure of a catalyst and the catalytic performance, its rational design remains a challenge.

Received: July 30, 2018
Revised: September 19, 2018
Published: September 21, 2018

DOI: 10.1021/acs.jpcc.8b07321
J. Phys. Chem. C 2018, 122, 23574−23581

One reason is the difficulty of the complete structural characterization of a catalyst, which requires state-of-the-art equipment (e.g., see van Bokhoven et al.[10] and Haber et al.[11]), but delivers only static, *postmortem* information. Dynamic information may be gained by comparison with kinetic measurements. True dynamic information requires *operando* methods, which are tailored to specific molecules, elements, and/or functional groups.[12−15] Because of its relevance, atomic probes have been developed giving insights into the schematic reaction mechanisms on the atomistic length- and time scale.[16−20] Recording nonperiodic, dynamic processes of technical catalysts with high spatial and temporal resolution on the mesoscopic scale is a particular challenge because the shorter the measurement interval, the lower the intensity, and the same is true for confining the length scale.[21] In addition to these challenges, the probing beam must be compatible to the harsh reaction conditions, for example, gas environment of the sample and temperature.[22,23] Recently, NMR methods have been developed with various applications in material sciences and chemical engineering.[24] Alternatively, microimaging by infrared (IR) microscopy can yield transient concentration profiles during catalytic conversion in nanoporous materials.[5]

Our approach is based on the interaction of neutrons with matter (mainly scattering), which is isotope-selective. The interaction of neutrons with many types of materials is relatively weak, and thus, for example, the neutron beam can easily penetrate thick aluminum walls of a chemical reactor. At the same time, neutrons have a large cross section with hydrogen, that is, we can follow the change in hydrogen concentration by means of neutron imaging in an operating chemical reactor (Figure 1). This technique has been used on a large scale to

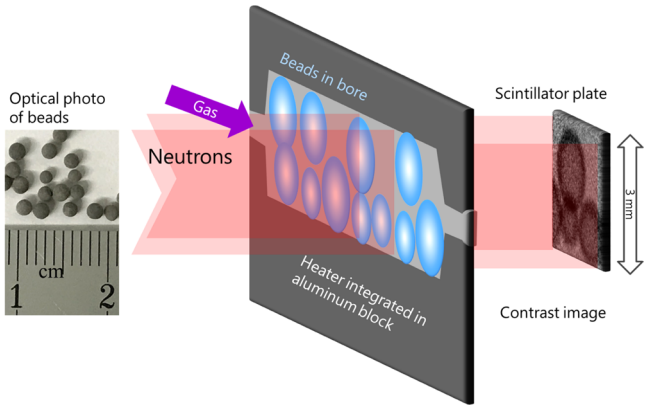

Figure 1. Sketch of the used setup: Left: Photograph of the studied catalyst beads. Right: The setup of cell and its orientation in the neutron beam.

study reactor kinetics to improve the reactor design and operation.[25] In this paper, we demonstrate the use of high-resolution neutron imaging as a local probe of the reaction mechanism on the sorption catalyst with a spatial and temporal resolution of 50 μm and 60 s, respectively, under reaction conditions, that is, hydrogen and carbon dioxide at ambient pressure and temperatures up to 300 °C.

The concept of sorption-enhanced catalysis[26] relies on the use of an appropriate support, such as a zeolite, which serves as an effective sink for specific products of the desired reaction, for example, water, thereby pushing the reaction in the direction of choice.[27] The model system for the methanation of CO_2 is nickel nanoparticles dispersed within the pores of a zeolite, which is known to readily absorb large quantities of water.[26,28]

$$CO_2 + 4H_2 + 2^* \rightarrow CH_4^{\uparrow} + 2H_2O^*,$$
$$\Delta H = -165\ \text{kJ / mol} + 2\Delta H_{ads} \quad (2)$$

The enthalpy of reaction is thus increased by the heat of water adsorption in the zeolite ΔH_{ads} as long as free adsorption sites (*) in the zeolite are available. In addition to the increase in the driving force, the water coverage of the catalytically active surfaces is reduced. As only methane leaves the catalyst, the number of water molecules in the catalyst increases over the course of reaction. This makes it an ideal model reaction for neutron imaging experiments, being sensitive to water.[25] At the same time, the product gas is analyzed by Fourier transform IR (FTIR) gas analysis. With this combination, we measure simultaneously the overall reaction and mesoscopic diffusion rate as required to derive the Thiele parameter. Although the system under investigation is very specific, the structure and dimensions are very typical for technical catalysts in general. The methodology is thus likely applicable to other catalytic systems.

EXPERIMENTAL SECTION

Samples. Nickel catalysts were supported on a commercial zeolite LTX (beads, 2 mm, Zeochem) by a wet impregnation process from a solution of nickel nitrate hexahydrate ($Ni(NO_3)_2{\cdot}6H_2O$, Sigma-Aldrich) in water. Therefore, the pure zeolites and the nickel nitrate hexahydrate powder were mixed, and water was added until complete dissolution of the nickel nitrate hexahydrate was achieved. The zeolite bead remained in the solution for several days. The impregnated zeolites were air-dried and reduced in a muffle furnace for 4 h (see also Delmelle et al.[28]). For characterization of nickel zeolites, see the Supporting Information.

Neutron Imaging. High-resolution neutron imaging[29−31] was applied on sorption catalysts made of Ni-impregnated 13× zeolite beads. Approximately 20 beads were placed in a heated reactor cell made of aluminum (see Figure 1). The experimental arrangement of the reactor allows resolving the water distribution in individual beads using the neutron contrast with the high-spatial resolution neutron imaging instrument (PSI Neutron Microscope). The high temperature of the reactor cell poses a challenge for the "Neutron Microscope" instrument. To prevent overheating and therefore degradation of the scintillator plate, the reactor cell is spatially separated from the scintillator plate. With this geometry at hand and the finite signal-to-noise ratio limited by the relatively short illumination time (1 min) for measuring kinetics, the effective spatial resolution of the neutron microscope is reduced to approximately 50 μm, as estimated from the images of steel screws in the direct vicinity of the catalyst beads (see the reactor in the Supporting Information). The image analysis was performed using the software ImageJ using built-in functions and a plug-in for image normalization developed by the Neutron Imaging and Applied Materials Group at PSI.[32] For details, see the Supporting Information.

Gas Supply and Analysis. The gas (reactants) flows were controlled by thermal mass flow meters from Bronkhorst connected to a Labview interface. Typical flow rates were 25 mL min^{-1} CO_2 and 100 mL min^{-1} H_2 (and deuterium). The product gases were led through an FTIR gas cell installed at a Bruker Alpha spectrometer acquiring spectra at a resolution of 0.8 cm^{-1}. The absorption of the IR radiation is used to measure

DOI: 10.1021/acs.jpcc.8b07321
J. Phys. Chem. C 2018, 122, 23574−23581

the concentration of CO_2 and CH_4 and the isotopomers of methane (see the Supporting Information).

RESULTS AND DISCUSSION

Water Distribution in Catalysts by Neutron Imaging.

As we are interested predominantly in water distribution in the catalyst beads, the images are normalized by a reference picture of the dry reactor giving the "background intensity" I_0. The deviation from the reference picture I_0/I is related to the local water content in the sample area expressed by a water "thickness" d by applying the Lambert–Beer law

$$\mu d = \ln\left(\frac{I_0}{I}\right) \tag{3}$$

The water content as depictively described by a thickness is easily converted into the total water content in the respective sample area by multiplying it with the sample area, for example, bead cross section (πr^2). This approach neglects the three-dimensional structure of the sample, in our case the curvature of a sphere. Locally resolved water *densities* have to be corrected to account for this (Supporting Information, water diffusion). Although the attenuation coefficient of neutrons for water by the thermal neutrons of the beamline used (POLDI, pulse overlap diffractometer) can be estimated (μ = 3.5 cm^{-1}),[33] we calibrate the setup by comparing the water uptake as measured by neutron imaging with uptake data measured thermogravimetrically on the same catalysts under identical conditions.

In Figure 2, the logarithmic neutron contrast of a bead upon exposure to a hydrogen gas stream with a partial water pressure

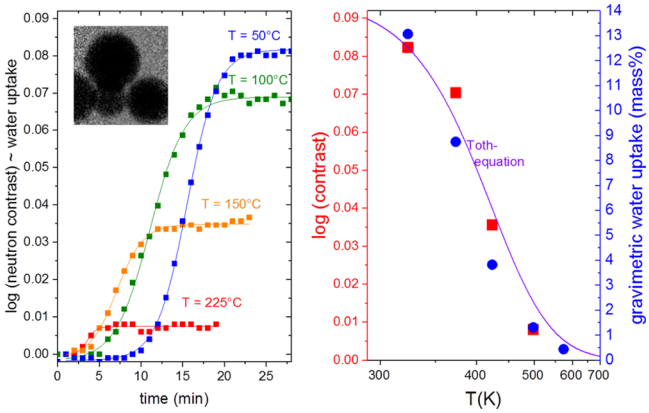

Figure 2. Left: Water uptake in Ni-zeolite 13× beads as measured by high-resolution neutron imaging. Right: The equilibrium values are compared to the water uptake as measured gravimetrically under identical conditions. The line is a fit to the Toth equations for pure zeolite 13× taken from ref 34 with one fit parameter considering the higher weight density because of the Ni content of the sorption catalyst.

of 6.5 mbar produced by a water humidifier is compared to the water uptake as measured gravimetrically. The total water uptake is a function of partial pressure and temperature; for zeolites, it is usually parametrized by the Toth equation (compare Wang and LeVan[34]). The sorption catalysts consist of a 13× zeolite with embedded Ni particles (see also the Supporting Information) with slightly different surface area and possibly modified sorbent–adsorbent interaction. The thermogravimetry data presented in Figure 2 match perfectly the literature data (Toth equation of pure 13× zeolite) after scaling by a factor considering the reduced surface area per weight. The integrated logarithm of the neutron contrast follows the same curve, and accordingly, a calibration curve is constructed from a direct comparison of the neutron contrast and thermogravimetry data without the knowledge of exact scattering coefficients and sample dimensions. Furthermore, the results shown in Figure 2 are a demonstration of the technique to measure gas–solid-phase diagrams.

Sorption kinetics are usually derived from modeling of experimental sorption uptake curves such as shown in Figure 2. This is due to the fact that many experimental techniques exist to measure such uptake/desorption curves (for an excellent introduction and overview, see Crank,[35] pages 160 ff and pages 246 ff), whereas methods visualizing temporally and spatially resolved diffusion processes are rare. The difficulty of modeling uptake curves is the experimental uncertainty: in general, uptake curves are very similar. However, the underlying mechanisms are derived from subtle quantitative differences, as kinetics hinge on details of the exact local conditions (time, partial pressures, gas, and sample temperature) and the exact geometry of the individual absorbing objects (e.g., bead diameter).[21]

The powerful feature of high-resolution neutron imaging is the provision of spatially resolved maps of the water distribution in the catalyst spheres. On the basis of such images, the kinetics of the water uptake can be readily investigated.

Without any preknowledge, the time-resolved high-resolution neutron images (see Figure 3) demonstrate the size dependence of the uptake in zeolite beads. A zone with high water content forms at the outer layer and grows with time. The center of small particles is reached earlier than that of larger particles, and saturation is reached earlier for the small particle. As expected, the corresponding uptake curves of the individual beads shown in Figure 3 differ markedly, that is, a smaller sphere is saturated faster than the larger one.

The time series of the neutron images was converted into the radial distribution of the water concentration in an individual bead (see the Supporting Information). Although in general a smooth concentration gradient is expected, the observed gradient is nearly step-like, which slowly moves into the center of the bead (so-called contracting envelope kinetics[36]). The diffusion constant of water in zeolites depends on the concentration,[21,37] which can be qualitatively understood by the fact that the adsorption enthalpy is concentration-dependent: water in a nearly empty zeolite is strongly bound than in a water saturated one. Thus, the interface between the surface with high water concentration and the region with very low water concentration acts as a barrier. The shape and propagation velocity of the moving interface determine the overall uptake kinetics.[36,38] Models based on measurements of the total uptake may give this insight, too, but have to consider the exact geometry of the absorbing medium (e.g., the size distribution of beads), which is usually not known in technical samples and may even change during operation because of mechanical stress. In addition, mass transport in technical materials takes place via extra- and intracrystalline diffusion.[21] A detailed analysis of the sorption phenomena will be published elsewhere.

A necessary condition of the method presented here to study dynamical phenomena is the spatial as well as temporal resolution. The radial distribution was discretized using Δr = 65 μm, and the time step was $\Delta\tau$ = 1 min. An estimation of the velocity of a (2D) diffusion front (see the Supporting Information) gives

DOI: 10.1021/acs.jpcc.8b07321
J. Phys. Chem. C 2018, 122, 23574–23581

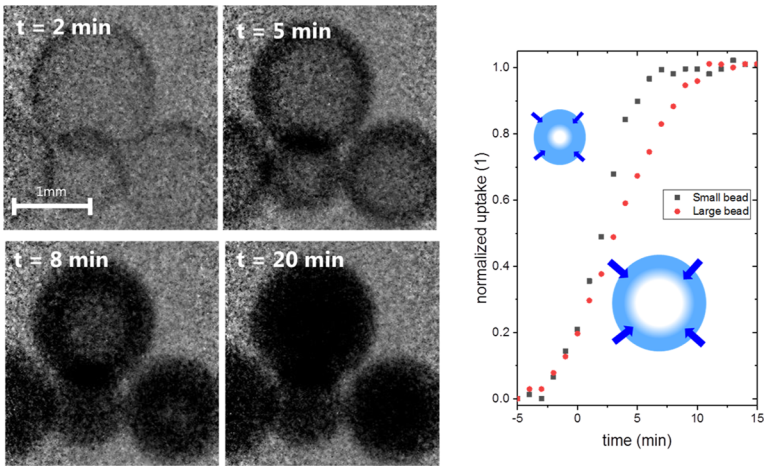

Figure 3. Left panel: Time series of high-resolution neutron images of the adsorption of water from humidified hydrogen gas. Temperature was 50 °C, water partial pressure was 6.5 mbar, and total flow was 100 mL min^{-1}. See the Supporting Information for quantification. Right panel: The normalized uptake of the individual catalyst grains as derived from the log of the integrated neutron attenuation (eq 3).

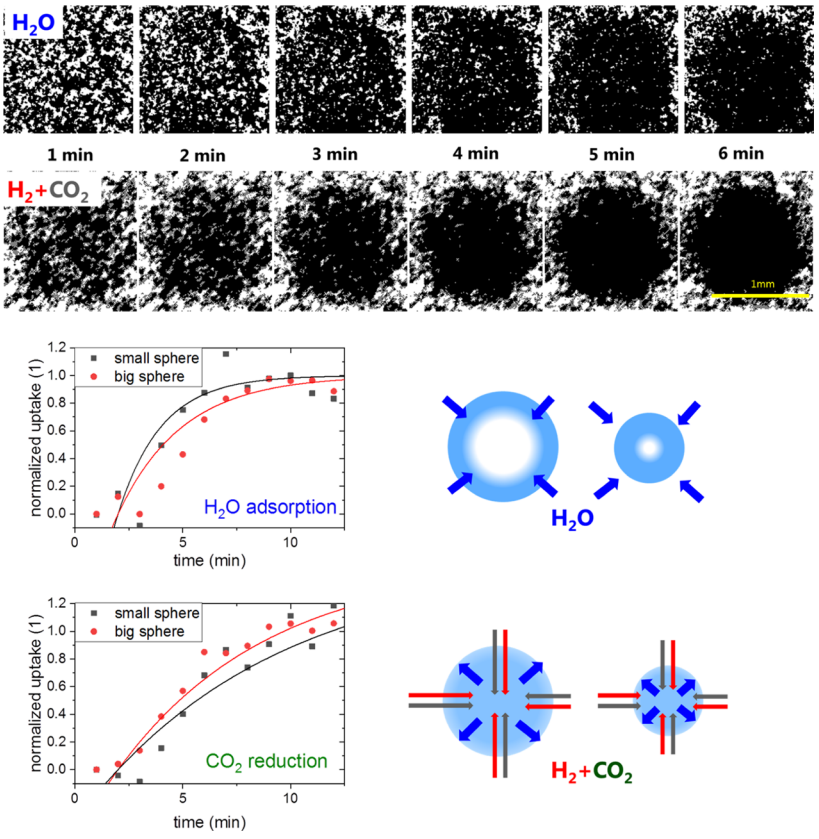

Figure 4. Time series of high-resolution neutron images showing water adsorption from a humidified hydrogen gas stream (top row) and water accumulation during sorption-enhanced methanation (bottom row). Temperature was 225 °C in both cases. Conditions for the water uptake humidified hydrogen gas flow with a water partial pressure of 6.5 mbar and a total flow of 100 mL min^{-1}, conditions for the reaction from 50 mL min^{-1} CO_2 and 200 mL min^{-1} H_2. Total uptake kinetics of catalyst beads during water uptake from adsorption of water from a humidified hydrogen gas (top panel) and from sorption-enhanced methanation (bottom panel) as derived from neutron images. The lines are fits to the function $f_i(t) = 1 - \exp\left[-\frac{t-t_0}{\tau_i}\right]$. The experimental time shift τ_0 is equal for all cases. From the initial slopes, reaction and diffusion rates may be estimated.

$$\frac{\Delta x}{\Delta t} \approx \sqrt{\frac{D}{t}} \tag{4}$$

which should be slower than the resolution ratio $\Delta r/\Delta t$. This means that diffusion fronts moving faster than this resolution ratio cannot be fully resolved, and the observation of local dynamic processes is limited to diffusion with an effective diffusion coefficient of $D \ll 10^{-9}$ m^2 s^{-1} for this particular experimental setup. One consequence of this estimation is that most of the dynamics studied in this publication cannot be resolved by that fine resolution, as most mechanisms are faster: the resolution of the diffusion process at 50 °C is just sufficient, and diffusion at higher temperatures and/or chemical reactions proceeds faster (see also the Supporting Information). For these

DOI: 10.1021/acs.jpcc.8b07321
J. Phys. Chem. C 2018, 122, 23574−23581

cases, we make use of the same strategy, shown in Figure 3, of following the total uptake kinetics of beads with different sizes. From a more general perspective, the estimation demonstrates the technical challenge associated with studying dynamical phenomena on a microscopic level: increasing the spatial resolution will only help, if the temporal resolution is equally increased. There are various possibilities to overcome this challenge: higher neutron flux, lower neutron energy because the cross section of neutrons for H in water increases with lower neutron energy,[39] and improved neutron detection.

Following the Sorption-Enhanced Methanation Reaction by Neutron Imaging. In this paper, we visualize a chemical reaction of choice (CO_2 methanation over supported nickel) inside such beads under reaction conditions. A significant reaction yield takes place above 225 °C only.[26,28] The indicator molecule is water: with each methane molecule, two water molecules are formed and accumulate inside the bead.

We compare the rate of water accumulation from the methanation reaction with that of water adsorption into the bead from a water-containing gas stream at the same temperature in Figure 4. Unlike during the adsorption of water from a water-containing gas stream, which shows the expected shell structure, water formed during the reaction accumulates homogeneously inside the bead, indicating that the catalysis of CO_2 methanation takes place throughout the bead simultaneously. This is in line of thought that the reaction rate is not limited by the diffusion of the reactants CO_2 and hydrogen but rate-limited by the surface reaction taking place on the active (Ni-) sites.

The maximum amount of water of the zeolite 13× is relatively small at 225 °C (Figure 2). This corresponds to a small neutron contrast and leads to relatively noisy images. To give further evidence of the conclusion, we apply the same strategy as used above: we measure the total uptake/reaction kinetics of individual beads with different sizes. As the measurements are made simultaneously, various experimental errors are equal and cancel out if the measurements are directly compared. Water uptake from a gas stream into a small bead is faster than into a large bead, which is also observed at this temperature (Figure 4). If the distribution of water inside the bead stemmed from evenly distributed reaction sites, the accumulation kinetics should not depend on size. This effect is indeed observed within the experimental error (Figure 4).

From a thermodynamical point of view, the sink of products pushing the equilibrium to the product side of the Sabatier reaction and the active site may be spatially separated. However, Figure 4 demonstrates good agreement with earlier studies[25] that at optimum reaction conditions, the rate of water formation in a bead by the reaction is faster than the water accumulation by diffusion in and out of the bead.[40] For slow reaction rates, the influence of diffusion is negligible, but at high reaction rates water diffusion is a relevant kinetic parameter. This means that the sorption enhancement is markedly reduced if the sorbent and catalyst are spatially separated because the water concentration at the catalytic reaction centers is high despite an overall low concentration.

The *operando* method presented here yields quantitative information supporting this qualitative statement. In contrast to model calculations, we measure the diffusion rate and effective reaction rate directly without special model assumptions. Initial rates of water uptake from the environment (i.e., the diffusion rate) are slightly lower than those of water accumulation by the reaction (i.e., effective reaction rate). With the catalyst dispersed inside the bead, water diffusion is irrelevant, and the reaction of CO_2 and hydrogen controls the overall reaction kinetics. As we cannot determine these diffusion rates directly, we estimate them from a comparison of the diffusion coefficients. Hydrogen diffusion is very fast with diffusion coefficients of around 10^{-8} m^2 s^{-1} at temperatures as low as 110 K.[41] CO_2 diffusion is slower and micropore diffusion is 1×10^{-14} m^2 s^{-1}, but here the relevant macropore diffusion is 3×10^{-6} m^2 s^{-1} at 343 K.[42,43] Combining the experimentally measured reaction and diffusion rates (from Figure 4), we estimate the rate-limiting diffusion rate by

$$r_{\mathrm{diff}}(\mathrm{CO_2}) = r_{\mathrm{diff}}(\mathrm{H_2O}) \cdot D(\mathrm{CO_2})/D(\mathrm{H_2O}) \tag{5}$$

yielding the Thiele parameter of the sorption catalyst

$$h_{\mathrm{T}}{}^2 = \frac{r_{\mathrm{reac}}}{r_{\mathrm{diff}}(\mathrm{H_2O}) \cdot \frac{D(\mathrm{CO_2})}{D(\mathrm{H_2O})}} = \frac{3 \times 10^{-3}\ \mathrm{s^{-1}}}{2 \times 10^{-3}\ \mathrm{s^{-1}} \cdot \frac{3 \times 10^{-6}}{4 \times 10^{-10}}} = 2 \times 10^{-4} \tag{6}$$

The reaction is thus clearly limited by catalysis. If the catalyst consisted of a spatially separated catalyst and sorbent, for example, the Ni catalyst as the outer shell of the bead, water diffusion would be rate-limiting and the Thiele parameter would be

$$h_{\mathrm{T}}{}^2 = \frac{r_{\mathrm{reac}}}{r_{\mathrm{diff}}(\mathrm{H_2O})} = \frac{3 \times 10^{-3}\ \mathrm{s^{-1}}}{2 \times 10^{-3}\ \mathrm{s^{-1}}} = 1.5 \tag{7}$$

The effectiveness factor of such catalyst geometry is nearly 1 for the nanostructured sorption catalyst and reduced to[4,44]

$$\eta = \frac{\tanh h_{\mathrm{T}}}{h_{\mathrm{T}}} = 0.6 \tag{8}$$

The parameter decreases quickly with increasing bead radius defining the diffusion path length in a physical mixture of the catalyst and pure zeolite beads. As a result, nanostructuring sorption catalysts by, for example, ion exchange in zeolite as utilized here to shorten the diffusion pathways is thus advantageous over physical mixtures with relatively long diffusion path lengths. It is recommended to the interested reader to compare the studies of Borgschulte et al.[45] with Walspurger et al.[46]

Following Methanation Reaction by Isotope Labelling. Water accumulation as an indicator for reaction kinetics is specific to sorption-enhanced reactions,[27] which include in addition to the discussed methanation reaction the reduction of CO_2 to CO and methanol, and possibly even the Fischer–Tropsch reaction, and dehydration reactions. However, in the majority of catalyzed reactions, the number of atoms in the catalyst bed remains constant after reaching steady state within short time, and as such neutron imaging is not easily applicable to other catalytic systems without sorption enhancement. This is also the case in a water-saturated sorption catalyst (see also the Supporting Information), where the role of the adsorptive medium is reduced to be the host of the catalyst particles.[26] To probe the dynamics of this state, a measurable neutron contrast is induced by abruptly exchanging hydrogen by deuterium during steady-state operation. The neutron cross section for deuterium is approximately 10 times smaller than that of protium.[47] Neglecting isotope effects, the chemical reaction continues to proceed irrespective of the isotope of hydrogen used. With the low neutron cross section of deuterium, we follow the formation of now deuterated water by a decrease in neutron

DOI: 10.1021/acs.jpcc.8b07321
J. Phys. Chem. C 2018, 122, 23574−23581

attenuation, in our neutron images indicated by a smaller relative contrast (Figure 5). The general concept is an established

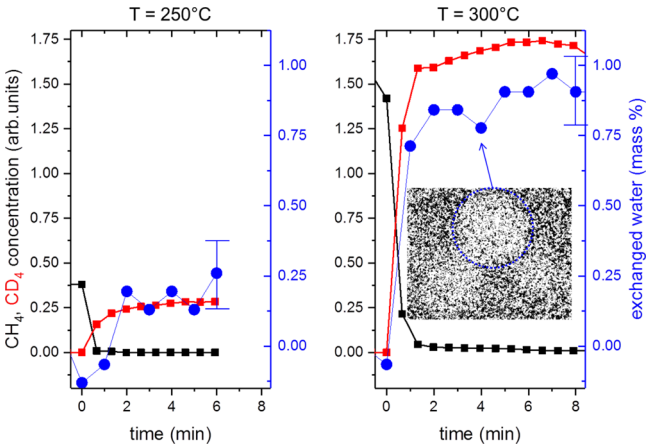

Figure 5. Left and right panels show the kinetics of methane and deuterated methane production after switching from hydrogen to deuterium during CO_2 conversion at 250 and 300 °C, respectively. At 250 °C, the neutron contrast is at the detection limit ($\Delta A/A = 6 \times 10^{-3}$), but the integrated signal shows a significant increase. At 300 °C, conversion and deuterium exchange in water of the zeolite is high enough to visualize the distribution.

approach in catalysis research [so-called steady-state isotopic transient kinetic analysis (SSITKA)[48]] with a beneficial side effect: the isotope labeling can be followed by IR spectroscopy in addition to neutron imaging because deuterated and hydrogenated carbon compounds can be easily distinguished by IR spectroscopy (see the Supporting Information, hydrogen–deuterium exchange).

At 250 °C, the catalytic conversion of CO_2 reduction to methane and deuterated methane, is near its maximum (see the Supporting Information, compare Borgschulte et al.[26]). The equilibrium levels of CH_4 and CD_4 concentrations in the exhaust stream reflect this dependence (Figure 5). The alteration of the exhaust composition from CH_4 to CD_4 as a result of switching of the reactant hydrogen to deuterium takes place within the time constant of the system[26] and can thus be considered instantaneous within the limits of the experiment. The reaction kinetics as a result of the gas composition is compared to the changes in the neutron contrast indicative of bulk exchange of H_2O to D_2O in the zeolite in Figure 5. Although hydrogen–deuterium gas exchange is fast at 250 °C on Ni surfaces,[49,50] the exchange of deuterium by hydrogen in methane in the observed bulk exchange as derived from integrated intensity changes is very small at this temperature. At 300 °C, bulk exchange is evident without further analysis from contrast changes of neutron microscopy images (see Figure 5). Main changes take place between the first two subsequent images in the acquired image series, that is, the reaction is instantaneous within the temporal and spatial resolution of the method of around 1 min and 50 μm, respectively. We do not observe a visible gradient. These observations are in perfect agreement with the state-of-the-art of this process: diffusion of hydrogen is orders of magnitude faster than that of water,[41,51] and thus, deuterium is practically instantaneously exchanged in the pores of the catalyst.

Bulk exchange of water in the zeolite crystals is possible by self-diffusion of a newly formed D_2O with already existing H_2O, which should also affect the neutron contrast. However, the amount of water in the zeolite is directly linked to gaseous water concentration, which is directly linked to the conversion yield: a 100% conversion results in a gaseous water concentration of 66 mol %. At 50% conversion, the water concentration drops to 25 mol %, and a similar dependence is found for the methane yield. Measuring the water concentration from a neutron contrast between hydrogen- and deuterium-labeled water yields thus the overall reaction yield as experimentally observed (Figure 5).

In general, the possibility of probing the time-dependent spatial distribution of reactants and products during catalysis is of great scientific and technologic interest. Recently, composites made of zeolites (HZSM-5) and In_2O_3 catalyst were found to show outstanding performance for methanol catalysis.[52] The empirical study highlights the importance of the mesoscopic structure without conclusive findings on the physical mechanism. More subtle phenomena as described by the Thiele parameter are expected to occur basically in every technical heterogeneous catalyst. Our method is ideally suited to study such systems down to tens of micrometer resolution. Enhanced spatial resolutions may be achieved using an optimized reaction cell/scintillator distance and/or by using highly collimated neutron beams. The current limit of the spatial and temporal resolutions given by the used detector is at about 5 μm and 1 ms.[29] The observed spatial and temporal resolutions in this study was 50 μm and 1 min. The spatial and temporal resolutions are interconnected and together limited by the density of protons in the sample and the available neutron flux. For providing higher spatial and temporal resolutions in future experiments, the alternatives are twofold: (i) utilization of the presented instrumentation in a higher neutron flux facilities and/or (ii) relaxing the spatial resolution requirements. Advances in neutron observations of processes using high-temporal resolution (with milliseconds exposure times) were recently shown in Trtik et al.[53] and Zboray et al.[54] The use of these techniques using hydrogen–deuterium exchange to induce a neutron contrast promises fascinating new results in the field of heterogeneous catalysis and beyond.

CONCLUSIONS

A time-resolved high-resolution neutron imaging has been utilized to noninvasively map the water concentration distribution inside catalyst beads catalyzing the sorption-enhanced CO_2 methanation reaction. The feasibility of temporal and spatial resolution of the method was demonstrated by following the water uptake in the sorption catalysts as measured by neutron imaging and gravimetric sorption analysis. The method reveals a wealth of data, including various new aspects of this model reaction system, and confirms some postulated and only indirectly evidenced hypotheses: we investigate the interplay of mass transport and catalytic reaction on a mesoscopic scale, from which the Thiele parameter of the catalytic system is derived. The low value of 2×10^{-4} confirms that nanostructuring sorption catalysts by, for example, ion exchange in zeolites as utilized here to shorten the diffusion pathways is advantageous over physical mixtures of catalysts and sorbents with relatively long diffusion path lengths. To envision the general applicability of the method, we follow the hydrogen–deuterium exchange reaction in the catalyst by neutron imaging combined with IR spectroscopy, a procedure, which is practicable for most hydrogen-based reactions.

DOI: 10.1021/acs.jpcc.8b07321
J. Phys. Chem. C 2018, 122, 23574–23581

■ ASSOCIATED CONTENT

Supporting Information

The Supporting Information is available free of charge on the ACS Publications website at DOI: 10.1021/acs.jpcc.8b07321.

Characterization of sorption catalyst, reactor setup and imaging processing, water uptake by gravimetric measurements, water diffusion, reaction kinetics my neutron microscopy, hydrogen−deuterium exchange by infrared spectroscopy (PDF)

■ AUTHOR INFORMATION

Corresponding Author

*E-mail: andreas.borgschulte@empa.ch. Phone.: +41 58 765 46 39. Fax: +41 58 765 40 22.

ORCID

Andreas Borgschulte: 0000-0001-6250-4667

Author Contributions

J.T., P.T., E.H.L., and A.B. designed and performed the experiments, R.D. and A.H. prepared the catalyst, M.H. characterized the catalysts, and all authors contributed to the evaluation and scientific discussion of the results. All authors have given approval to the final version of the manuscript.

Notes

The authors declare no competing financial interest.

■ ACKNOWLEDGMENTS

This work was partly supported by the UZH-UFSP program LightChEC. Financial support from BFE and FOGA (SmartCat project) and the Swiss National Science Foundation (grant nos. 144120 and 172662) is acknowledged.

■ ABBREVIATIONS

FTIR, Fourier transform infrared; SSITKA, steady-state isotopic transient kinetic analysis; POLDI, pulse overlap diffractometer

■ REFERENCES

(1) Bartholomew, C. H.; Farrauto, R. J. Introduction and Fundamentals. *Fundamentals of Industrial Catalytic Processes*; John Wiley & Sons, Inc.: Hoboken, New Jersey, 2006; pp 3−59.

(2) Wintterlin, J.; Völkening, S.; Janssens, T. V. W.; Zambelli, T.; Ertl, G. Atomic and Macroscopic Reaction Rates of a Surface-Catalyzed Reaction. *Science* **1997**, *278*, 1931−1934.

(3) Bartholomew, C. H.; Farrauto, R. J. Catalyst Materials, Properties and Preparation. *Fundamentals of Industrial Catalytic Processes*; John Wiley & Sons, Inc.: Hoboken, New Jersey, 2006; pp 60−117.

(4) Thiele, E. W. Relation between Catalytic Activity and Size of Particle. *Ind. Eng. Chem.* **1939**, *31*, 916−920.

(5) Titze, T.; Chmelik, C.; Kullmann, J.; Prager, L.; Miersemann, E.; Gläser, R.; Enke, D.; Weitkamp, J.; Kärger, J. Microimaging of Transient Concentration Profiles of Reactant and Product Molecules during Catalytic Conversion in Nanoporous Materials. *Angew. Chem. Int. Ed.* **2015**, *54*, 5060−5064.

(6) Hill, C. G.; Root, T. W. *Introduction to Chemical Engineering Kinetics and Reactor Design*; John Wiley & Sons, Inc.: Hoboken, New Jersey, 2014.

(7) Becker, H.; Güttel, R.; Turek, T. Enhancing internal mass transport in Fischer-Tropsch catalyst layers utilizing transport pores. *Catal. Sci. Technol.* **2016**, *6*, 275−287.

(8) Smit, B.; Maesen, T. L. M. Towards a Molecular Understanding of Shape Selectivity. *Nature* **2008**, *451*, 671−678.

(9) van Santen, R. A.; Markvoort, A. J.; Ghouri, M. M.; Hilbers, P. A. J.; Hensen, E. J. M. Monomer Formation Model versus Chain Growth Model of the Fischer-Tropsch Reaction. *J. Phys. Chem. C* **2013**, *117*, 4488−4504.

(10) van Bokhoven, J. A.; Lamberti, C. XAS Techniques to Determine Catalytically Active Sites in Zeolites: The Case of Cu-Zeolites. In *XAFS Techniques for Catalysts, Nanomaterials, and Surfaces*; Iwasawa, Y., Asakura, K., Tada, M., Eds.; Springer International Publishing: Cham, Switzerland, 2017; pp 299−316.

(11) Haber, J.; Block, J. H.; Delmon, B. Methods and Procedures for Catalyst Characterization. *Handbook of Heterogeneous Catalysis*; Wiley-VCH Verlag GmbH & Co. KGaA, 2008; pp 1230−1258.

(12) Weitz, E. New Physical Insights in Experimental Studies in Catalysis. *J. Phys. Chem. C* **2017**, *121*, 23852.

(13) Newton, M. A.; Dent, A. J. Energy-Dispersive EXAFS: Principles and Application in Heterogeneous Catalysis. In *In situ Characterization of Heterogeneous Catalysts*; Rodriguez, J. A., Hanson, J. C., Chupas, P. J., Eds.; John Wiley & Sons, Inc.: Hoboken, New Jersey, 2013; pp 75−119.

(14) Newton, M. A.; Ferri, D.; Smolentsev, G.; Marchionni, V.; Nachtegaal, M. Kinetic Studies of the Pt Carbonate-Mediated, Room-Temperature Oxidation of Carbon Monoxide by Oxygen over Pt/Al2O3 Using Combined, Time-Resolved XAFS, DRIFTS, and Mass Spectrometry. *J. Am. Chem. Soc.* **2016**, *138*, 13930−13940.

(15) Frenken, J.; Groot, I. *Operando Research in Heterogeneous Catalysis*; Springer International Publishing: Cham, Switzerland, 2017.

(16) Zaera, F. Outstanding Mechanistic Questions in Heterogeneous Catalysis. *J. Phys. Chem. B* **2002**, *106*, 4043−4052.

(17) Salmeron, M.; Schlogl, R. Ambient Pressure Photoelectron Spectroscopy: A New Tool for Surface Science and Nanotechnology. *Surf. Sci. Rep.* **2008**, *63*, 169−199.

(18) Behrens, M.; Studt, F.; Kasatkin, I.; Kuhl, S.; Havecker, M.; Abild-Pedersen, F.; Zander, S.; Girgsdies, F.; Kurr, P.; Kniep, B.-L.; et al. The Active Site of Methanol Synthesis over Cu/ZnO/Al2O3 Industrial Catalysts. *Science* **2012**, *336*, 893−897.

(19) Matthiesen, J.; Wendt, S.; Hansen, J. Ø.; Madsen, G. K. H.; Lira, E.; Galliker, P.; Vestergaard, E. K.; Schaub, R.; Lægsgaard, E.; Hammer, B.; et al. Observation of All the Intermediate Steps of a Chemical Reaction on an Oxide Surface by Scanning Tunneling Microscopy. *ACS Nano* **2009**, *3*, 517−526.

(20) Zewail, A. H. Femtochemistry: Atomic-Scale Dynamics of the Chemical Bond Using Ultrafast Lasers (Nobel Lecture). *Angew. Chem. Int. Ed.* **2000**, *39*, 2586−2631.

(21) Kärger, J.; Ruthven, D. M. Diffusion in Nanoporous Materials: Fundamental Principles, Insights and Challenges. *New J. Chem.* **2016**, *40*, 4027−4048.

(22) Imbihl, R.; Behm, R. J.; Schlögl, R. Bridging the Pressure and Material Gap in Heterogeneous Catalysis. *Phys. Chem. Chem. Phys.* **2007**, *9*, 3459.

(23) Delmelle, R.; Probst, B.; Alberto, R.; Züttel, A.; Bleiner, D.; Borgschulte, A. Closing the Pressure Gap in X-Ray Photoelectron Spectroscopy by Membrane Hydrogenation. *Rev. Sci. Instrum.* **2015**, *86*, 053104.

(24) Koptyug, I. V. Magnetic Resonance Imaging Methods in Heterogeneous Catalysis. *Spectrosc. Prop. Inorg. Organomet. Compd.* **2014**, *45*, 1−42.

(25) Borgschulte, A.; Delmelle, R.; Duarte, R. B.; Heel, A.; Boillat, P.; Lehmann, E. Water Distribution in a Sorption Enhanced Methanation Reactor by Time Resolved Neutron Imaging. *Phys. Chem. Chem. Phys.* **2016**, *18*, 17217−17223.

(26) Borgschulte, A.; Gallandat, N.; Probst, B.; Suter, R.; Callini, E.; Ferri, D.; Arroyo, Y.; Erni, R.; Geerlings, H.; Züttel, A. Sorption enhanced CO2 methanation. *Phys. Chem. Chem. Phys.* **2013**, *15*, 9620−9625.

(27) Carvill, B. T.; Hufton, J. R.; Anand, M.; Sircar, S. Sorption-enhanced reaction process. *AIChE J.* **1996**, *42*, 2765−2772.

(28) Delmelle, R.; Duarte, R. B.; Franken, T.; Burnat, D.; Holzer, L.; Borgschulte, A.; Heel, A. Development of improved nickel catalysts for sorption enhanced CO 2 methanation. *Int. J. Hydrogen Energy* **2016**, *41*, 20185−20191.

DOI: 10.1021/acs.jpcc.8b07321
J. Phys. Chem. C 2018, 122, 23574−23581

(29) Trtik, P.; Lehmann, E. H. Progress in High-Resolution Neutron Imaging at the Paul Scherrer Institut - The Neutron Microscope Project. *J. Phys.: Conf. Ser.* **2016**, *746*, 012004.
(30) Trtik, P.; Hovind, J.; Grünzweig, C.; Bollhalder, A.; Thominet, V.; David, C.; Kaestner, A.; Lehmann, E. H. Improving the Spatial Resolution of Neutron Imaging at Paul Scherrer Institut - The Neutron Microscope Project. *Phys. Procedia* **2015**, *69*, 169−176.
(31) Kaestner, A. P.; Trtik, P.; Zarebanadkouki, M.; Kazantsev, D.; Snehota, M.; Dobson, K. J.; Lehmann, E. H. Recent Developments in Neutron Imaging with Applications for Porous Media Research. *Solid Earth* **2016**, *7*, 1281−1292.
(32) Rasband, W. S. ImageJ (incl. plugins for image referencing developed and provided by members of Paul Scherrer Institut, Villigen/Aargau, Switzerland). https://imagej.nih.gov/ij/index.html (accessed March 1, 2018).
(33) O'Brien, J. *DOE Fundamentals Handbook, Nuclear Physics and Reactor Theory*, DOE-HDBK-1019/1-93; U.S. Department of Energy, 1993.
(34) Wang, Y.; LeVan, M. D. Adsorption Equilibrium of Carbon Dioxide and Water Vapor on Zeolites 5A and 13X and Silica Gel: Pure Components. *J. Chem. Eng. Data* **2009**, *54*, 2839−2844.
(35) Crank, J. *The Mathematics of Diffusion*; Clarendon Press: Oxford, 1975.
(36) Mintz, M. H.; Zeiri, Y. Hydriding Kinetics of Powders. *J. Alloys Compd.* **1995**, *216*, 159−175.
(37) Demontis, P.; Suffritti, G. B.; Fois, E. S.; Quartieri, S. Molecular Dynamics Studies on Zeolites. 6. Temperature Dependence of Diffusion of Methane in Silicalite. *J. Phys. Chem.* **1992**, *96*, 1482−1490.
(38) Koptyug, I. V.; Khitrina, L. Y.; Aristov, Y. I.; Tokarev, M. M.; Iskakov, K. T.; Parmon, V. N.; Sagdeev, R. Z. An1H NMR Microimaging Study of Water Vapor Sorption by Individual Porous Pellets. *J. Phys. Chem. B* **2000**, *104*, 1695−1700.
(39) Horsley, A. Neutron Cross Sections of Hydrogen in the Energy Range 0.0001 EV − 20 MeV. *Nucl. Data* **1966**, *2*, 243−262.
(40) Delmelle, R.; Terreni, J.; Remhof, A.; Heel, A.; Proost, J.; Borgschulte, A. Evolution of Water Diffusion in a Sorption-Enhanced Methanation Catalyst. *Catalysts* **2018**, *8*, 341.
(41) Bär, N.-K.; Ernst, H.; Jobic, H.; Kärger, J. Combined Quasi-Elastic Neutron Scattering and NMR Study of Hydrogen Diffusion in Zeolites. *Magn. Reson. Chem.* **1999**, *37*, S79−S83.
(42) Kamiuto, K.; Goubaru, A.; Ermalina. Diffusion Coefficients of Carbon Dioxide within Type 13X Zeolite Particles. *Chem. Eng. Commun.* **2006**, *193*, 628−638.
(43) Ahn, H.; Moon, J.-H.; Hyun, S.-H.; Lee, C.-H. Diffusion Mechanism of Carbon Dioxide in Zeolite 4A and CaX Pellets. *Adsorption* **2004**, *10*, 111−128.
(44) Hegedus, L. L.; Petersen, E. E. The Single Pellet Diffusion Reactor: Theory and Applications. *Catal. Rev.* **1974**, *9*, 245−266.
(45) Borgschulte, A.; Callini, E.; Stadie, N.; Arroyo, Y.; Rossell, M. D.; Erni, R.; Geerlings, H.; Züttel, A.; Ferri, D. Manipulating the Reaction Path of the CO_2 Hydrogenation Reaction in Molecular Sieves. *Catal. Sci. Technol.* **2015**, *5*, 4613−4621.
(46) Walspurger, S.; Elzinga, G. D.; Dijkstra, J. W.; Sarić, M.; Haije, W. G. Sorption Enhanced Methanation for Substitute Natural Gas Production: Experimental Results and Thermodynamic Considerations. *Chem. Eng. J.* **2014**, *242*, 379−386.
(47) Sears, V. F. Neutron Scattering Lengths and Cross Sections. *Neutron News* **1992**, *3*, 26−37.
(48) Ledesma, C.; Yang, J.; Chen, D.; Holmen, A. Recent Approaches in Mechanistic and Kinetic Studies of Catalytic Reactions Using SSITKA Technique. *ACS Catal.* **2014**, *4*, 4527−4547.
(49) Shooter, D.; Farnsworth, H. E. Hydrogen-Deuterium Exchange on Clean Nickel Surfaces. *J. Phys. Chem. Solids* **1961**, *21*, 219−227.
(50) Johansson, M.; Lytken, O.; Chorkendorff, I. The Sticking Probability for H_2 on Some Transition Metals at a Hydrogen Pressure of 1 Bar. *J. Chem. Phys.* **2008**, *128*, 034706.
(51) Kärger, J.; Vasenkov, S.; Auerbach, S. M. Diffusion in Zeolites. In *Handbook of Zeolite Science and Technology*; Auerbach, S. M., Carrado, K. A., Dutta, P. K., Eds.; CRC Press: Boca Raton, 2003; pp 446−548.
(52) Gao, P.; Li, S.; Bu, X.; Dang, S.; Liu, Z.; Wang, H.; Zhong, L.; Qiu, M.; Yang, C.; Cai, J.; et al. Direct conversion of CO2 into liquid fuels with high selectivity over a bifunctional catalyst. *Nat. Chem.* **2017**, *9*, 1019−1024.
(53) Trtik, P.; Morgano, M.; Bentz, R.; Lehmann, E. 100 Hz Neutron Radiography at the BOA Beamline Using a Parabolic Focussing Guide. *MethodsX* **2016**, *3*, 535−541.
(54) Zboray, R.; Trtik, P. 800 Fps Neutron Radiography of Air-Water Two-Phase Flow. *MethodsX* **2018**, *5*, 96−102.

DOI: 10.1021/acs.jpcc.8b07321
J. Phys. Chem. C 2018, 122, 23574−23581